The Added Value of Statistical Modeling of Backscatter Properties in the Management of Breast Lesions at US[1]

Isabelle Trop, MD, MPH
François Destrempes, PhD, PhD
Mona El Khoury, MD
André Robidoux, MD
Louis Gaboury, MD
Louise Allard, PhD
Boris Chayer, MEng
Guy Cloutier, Eng, PhD

Purpose: To develop a classification method based on the statistical backscatter properties of tissues that can be used as an ancillary tool to the usual Breast Imaging Reporting and Data System (BI-RADS) classification for solid breast lesions identified at ultrasonography (US).

Materials and Methods: This study received institutional review board approval, and all subjects provided informed consent. Eighty-nine women (mean age, 50 years; age range, 22–82 years) with 96 indeterminate solid breast lesions (BI-RADS category 4–5; mean size, 13.2 mm; range, 2.6–44.7 mm) were enrolled. Prior to biopsy, additional radiofrequency US images were obtained, and a 3-second cine sequence was used. The research data were analyzed at a later time and were not used to modify patient management decisions. The lesions were segmented manually, and parameters of the homodyned K distribution (α, k, and μ_n values) were extracted for three regions: the intratumoral zone, a 3-mm supratumoral zone, and a 5-mm infratumoral zone. The Mann-Whitney rank sum test was used to identify parameters with the best discriminating value, yielding intratumoral α, supratumoral k, and infratumoral μ_n values.

Results: The 96 lesions were classified as follows: 48 BI-RADS category 4A lesions, 16 BI-RADS category 4B lesions, seven BI-RADS category 4C lesions, and 25 BI-RADS category 5 lesions. There were 24 cancers (25%). The area under the receiver operating characteristic curve was 0.76 (95% confidence interval: 0.65, 0.86). Overall, 24% of biopsies (in 17 of 72 lesions) could have been spared. By limiting analysis to lesions with a lower likelihood of malignancy (BI-RADS category 4A–4B), this percentage increased to 26% (16 of 62 lesions). Among benign lesions, the model was used to correctly classify 10 of 38 fibroadenomas (26%) and three of seven stromal fibroses (43%).

Conclusion: The statistical model performs well in the classification of solid breast lesions at US, with the potential of preventing one in four biopsies without missing any malignancy.

©RSNA, 2014

Radiology

Breast ultrasonography (US) is the diagnostic modality of choice to characterize solid lesions, but this technique remains operator dependent. B-mode gray-scale US can be used to categorize solid lesions according to their morphologic features (1), allowing classification into Breast Imaging Reporting and Data System (BI-RADS) categories according to the risk of malignancy (2). In the evaluation of women with an increased risk of breast cancer, combining US with mammography yielded a sensitivity of 89% for breast cancer detection but a moderate specificity of 71% (3). Lesions classified in BI-RADS categories 4 or 5 undergo biopsy so that all cancers in this subgroup are identified, within the limits of sampling error and pathologic assessment accuracy, which is equivalent to a sensitivity of 100%. On the other hand, many biopsies confirm the absence of cancer.

Much research has been conducted in the search for additional parameters that may help classify solid lesions at US. Some avenues explored include evaluation of lesion vascularity through Doppler techniques, with or without contrast material enhancement, which have met with limited success (4–6). A promising field is US elastography, which is based on the detection of areas of tissue stiffness. Initial efforts involved compression elastography, but this approach is receiving less attention because of substantial interobserver variability inherent to the technique, which requires

manual compression, and its limited performance for deep lesions (7–10). Dynamic elastography is used to estimate tissue stiffness by tracking shear waves induced by radiation pressure–transmitted echoes (11–14): It is minimally operator dependent and comparable to the BI-RADS classification in its accuracy (15).

Another avenue to help characterize breast lesions is the analysis of echo signals arising from US wave interferences with a given lesion. The statistical nature of these echoes can be explored for tissue characterization. To date, different statistical distribution models have been proposed for breast imaging: the K distribution (16) and the Nakagami distribution (17–20), with a third model, the homodyned K distribution, having thus far only been used to investigate mice mammary tumors (21,22) and human lymph nodes (23). In the present study, we adopted the homodyned K model because it is a more general and complete model than the K or Nakagami distributions. Indeed, neither the K nor the Nakagami distribution fully captures the cellular organization of the nuclei: The K distribution assumes a vanishing coherent component (ie, no structured cellular organization), whereas the Nakagami distribution is based on only one shape parameter that combines the spatial organization of the nuclei on one hand and their number and homogeneity of their cross-sections on the other hand, but without quantifying these two aspects separately (24). We hypothesized that US signal envelope statistics could provide a cellular signature of breast tumors (ie, size, spatial organization, density, and acoustic properties of the cells forming the lesion and its surrounding tissues), demonstrating

information that could potentially be used to differentiate benign from malignant lesions. The aim of this study was to develop a classification method based on the statistical backscatter properties of tissues that can be used as an ancillary tool to the usual BI-RADS classification for solid breast lesions identified at US.

Materials and Methods

This study was approved by our institutional review board, and all subjects gave written informed consent.

Patient Selection

Women were selected who were examined at our breast imaging center and had a solid lesion at B-mode US (referred to as "standard US"), for which biopsy was recommended (BI-RADS categories 4 and 5), with no other solid lesion in the quadrant of interest and no prior surgery or biopsy in the breast of interest. The women selected were offered participation in this study; consent was granted by all participants approached. Women with breast implants were excluded.

US Imaging and Experiments

Breast lesions were initially evaluated per standard clinical practice by one of two fellowship-trained breast radiologists (I.T. and M.E.K., with 11 and 8 years of

Advance in Knowledge

- The proposed model of Statistical Tissue Characterization (STC) based on US backscatter properties of solid breast lesions can be used to classify Breast Imaging Reporting and Data System (BI-RADS) category 4–5 lesions as benign or malignant with 100% sensitivity (24 of 24 lesions), 24% specificity (17 of 72 lesions), and an area under the receiver operating characteristic curve of 0.76 (95% confidence interval: 0.65, 0.86).

Implication for Patient Care

- Complementary analysis with the proposed STC model can be used to prevent 26% of biopsies (in 16 of 62 lesions) initially recommended for BI-RADS category 4A and 4B lesions later confirmed to be benign, potentially without missing any malignant lesion.

practice, respectively) with a conclusive BI-RADS assessment based on clinical, mammographic, and B-mode US features. B-mode standard US evaluations were performed with a Logiq 9 system (General Electric Healthcare, Mississauga, Ontario, Canada). For women who gave informed consent, prior to biopsy, additional radiofrequency (RF) images were obtained by using B-mode guidance with a Terason t3000 US scanner (Teratech, Burlington, Mass), referred to as "backscatter US." For each lesion, a longitudinal 3-second cine sequence with a mean frame rate of 32 Hz was performed with a fixed default setting (medium size, nominal center frequency of 7.1 MHz, focused at 2 cm, bandwidth of 40%, depth of 4 cm, and lateral and axial discretizations of 0.1545 mm per pixel and 0.0208 mm per pixel, respectively). The echo envelope was computed from RF data as described previously (25) by using MatLab software (MathWorks, Natick, Mass); no filters or log compression were applied except for display purposes. For each lesion, breast quadrant location, depth, size, and BI-RADS assessment were recorded. When mammographic evaluation was also available, breast density was recorded in one of four categories (fatty, scattered areas of fibroglandular tissue density, heterogeneously dense, or extremely dense) per the BI-RADS nomenclature (2).

Percutaneous US-guided biopsy was performed after administration of local anesthesia with Xylocaine 1% (Alveda Pharmaceuticals, Toronto, Ontario, Canada), by using 14- or 16-gauge core needles and a Manan Pro-Mag 2.2 biopsy gun (Medical Device Technologies, Gainesville, Fla); three to seven cores were obtained per lesion, at the radiologist's discretion.

Breast pathologists performed histopathologic analyses. Final diagnoses were categorized as benign or malignant; for this study, atypia was considered a benign diagnosis. The label "fibrocystic changes" was applied to group all lesions with pathologic diagnoses that included sclerosing adenosis, apocrine metaplasia, ductal hyperplasia, and sclerocystic changes. Patient management decisions

were made per usual clinical practice, without consideration of the RF data obtained from the backscatter US.

Lesion Analysis

The RF data were transferred to a workstation for analysis; lesions were labeled with a numeric code that did not reveal patient identity or lesion characteristics. The contour of each lesion was manually drawn (segmentation) on the first frame of each image sequence by a breast radiologist (I.T.) (Fig 1) a mean of 93 days (range, 30–263 days) after the acquisition, after which segmentation was automatically propagated along remaining frames of the sequence with motion compensation by using an algorithm described previously (26). Two additional regions of interest (ROIs) were defined: a 3-mm-thick supratumoral zone right above the lesion and a 5-mm-thick infratumoral zone right below the lesion (Fig 1). These two zones were defined to take into account alterations in peritumoral tissues that may result from extension and reaction of surrounding parenchyma to malignant cells (spiculations, formation of an echogenic rim); in addition to the 3-mm supratumoral zone, a slightly larger 5-mm infratumoral zone was created to include posterior shadowing features associated with malignancy, when present. These two ROIs were automatically computed on the basis of the contours of the segmented lesion. There were 15 of 96 superficial lesions (16%) and one of 96 deep lesions (1%) for which a less-than-3-mm supratumoral zone and less-than-5-mm infratumoral zone, respectively, were used.

For each of these three ROIs, the amplitude (gray level) of the echo envelope reconstructed from RF signals acquired with the backscatter US method was modeled by a homodyned K distribution (27). Three parameters with a physical meaning were derived: *(a)* The scattering clustering parameter α, reflecting the number of scatterers (cellular nuclei) within the resolution range and the homogeneity of their cross-sections; *(b)* the total signal power μ_n normalized by the maximum intensity in the ROI (expressed

on a scale of 0 to 1000), clinically akin to B-mode echogenicity; and *(c)* the coherent-to-diffuse signal ratio k, which reflects the cellular spatial organization of the nuclei. The parameters were estimated on each frame of the 3-second cine sequence, and the mean values over the frames were adopted as estimators (27). Lesion analyses were performed by using computer programs in C++, except for the manual segmentations that were based on a program written with MatLab (MathWorks).

Data Analysis

The Mann-Whitney rank sum test was used to identify which of the α, μ_n, and k parameters of the homodyned K distribution yielded the lowest P value (thus viewed as a cost function) between benign and malignant lesions for each ROI. These analyses were performed by using SigmaStat (Systat Software, San Jose, Calif).

By adopting a leave-one-patient-out cross-validation scheme, each of the 96 lesions was tested while the lesions of remaining patients were used to train the tested classification scheme. For each training set, thresholds were calculated for each parameter by considering a multiple t of its standard deviation on the class of malignant lesions in the training set. The value $t = 2.94$ yielded one-sided intervals for the three classifying parameters with a combined 99.5% confidence level after Bonferroni correction. A tested lesion was considered malignant if all the following conditions were satisfied: *(a)* The supratumoral k value was superior to the mean $(k) - t$ standard deviation (k); *(b)* the intratumoral α value was inferior to the mean $(\alpha) + t$ standard deviation (α); and *(c)* the infratumoral μ_n value was inferior to the mean $(\mu_n) + t$ standard deviation (μ_n), where the means and standard deviations of the parameters were estimated on the training data. On the other hand, if any of the parameters fell outside of one of these one-sided confidence intervals, the lesion was classified as benign according to the model.

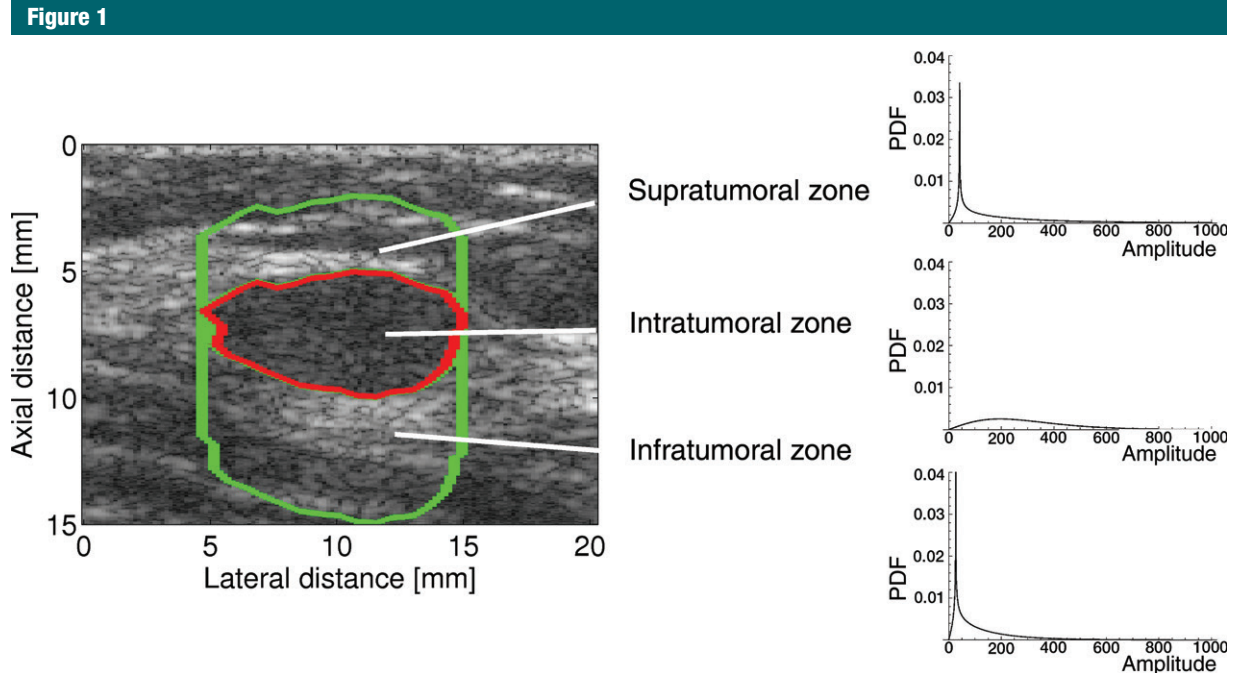The sensitivity and specificity were computed by summing true and false

Figure 1

Figure 1: B-mode US image (left) of a fibroadenoma with its corresponding homodyned *K* distributions (right) in a 31-year-old woman. A solid lesion was identified and was subsequently confirmed with biopsy to be a benign fibroadenoma. Segmentation of the lesion (red contours) was performed manually, and the supratumoral and infratumoral zones (green contours) were automatically calculated. This was then automatically propagated along the remaining frames of the sequence. From the distribution of echoes on the B-mode US image, probability density functions *(PDF)* of homodyned *K* distributions were estimated from each zone of the lesion.

positive and negative findings over the 96 tested lesions. A receiver operating characteristic (ROC) curve was computed by varying *t* values. Two thousand stratified bootstraps of the patients (these are default settings of the free R statistical software, R Foundation, Vienna Austria) and computations of the area under the curve (with the trapezoidal method) of the resulting ROC curves based on a leave-one-patient-out cross-validation scheme (in all lesions of the resampled patients for each bootstrap) were used to estimate the median and the 95% confidence interval of the area under the curve. Sensitivity and specificity were also calculated in the subgroup of BI-RADS category 4A and 4B lesions. These analyses were conducted by using Mathematica software (Wolfram Research, Champaign, Ill).

To address the sensitivity of the proposed Statistical Tissue Characterization (STC) method for manual delineation of lesion contours in the first frame of the cine loops, the control points of the manually drawn contours were randomly modified within radii of 0.5, 1.0, and 1.5 mm. The performance of the STC method was then re-evaluated with the leave-one-patient-out cross-validation scheme for all sequences but by using the randomly modified initial contours whenever testing a lesion.

Results

Study Population

Between April 2010 and December 2011, longitudinal cine sequences were performed prospectively in 89 women with 96 lesions; seven women had two lesions. The mean patient age was 50 years (range, 22–82 years). Forty-eight women had undergone menopause; five had previously been treated for contralateral breast cancer, and two

were pregnant at the time of biopsy. Of 80 women with available mammography findings, 50 (62%) had moderate to high breast density.

Breast Lesions

Fifty-two of 96 lesions (54%) were in the right breast, and 44 (46%) were in the left breast. Most lesions were in the upper outer quadrants: 24 of 44 (54%) were located on the left side, and 26 of 52 (50%) were located on the right side. The longest lesion diameter ranged from 2.6 to 44.7 mm (mean, 13.2 mm; median, 10.9 mm); five of 96 lesions (5%) measured up to 5 mm in size. Position within the breast was classified as the deepest third of the breast for 18 lesions (19%), the middle third of the breast for 51 lesions (53%), and the superficial third of the breast for 27 lesions (28%). Seventy-one of 96 solid lesions (74%) were classified at standard US as being moderately suspicious for malignancy: 48 lesions were classified as BI-RADS

Table 1

BI-RADS Assessment after Standard US Evaluation versus the STC Model

BI-RADS Category after Standard US Evaluation	No. of Lesions	Rate of Malignancy (%)	No. of Benign Lesions	No. of Lesions Classified as Benign according to Each Parameter			Rate of True-Negative Findings based on the STC Model (%)
				Supratumoral k	Intratumoral α	Infratumoral μ_n	
4A	48	0	48	5	3	3	23 (11/48)
4B	16	12 (2/16)	14	1	3	1	36 (5/14)
4C	7	28 (2/7)	5	0	1	0	20 (1/5)
5	25	80 (20/25)	5	0	0	0	0 (0/5)
Total	96	25 (24/96)	72	6	7	4	24 (17/72)

Note.—Numbers in parentheses are the data used to calculate percentages.

Table 2

STC Model Performance for Benign Lesions versus Specific Lesion Type

Lesion Type	No. of Lesions	Mean Size (mm)	No. of Lesions Classified as Benign according to Each Parameter			Rate of True-Negative Findings (%)
			Supratumoral k	Intratumoral α	Infratumoral μ_n	
Fibroadenoma	38	15.4	5	4	1	26 (10/38)
Fibrocystic changes	20	10.8	1	1	1	15 (3/20)
Stromal fibrosis	7	7.8	0	2	1	43 (3/7)
Papillary lesions	5	9.1	0	0	1	20 (1/5)
Other (one radial scar, one angiolipoma)	2	7.5	0	0	0	0 (0/2)

Note.—Numbers in parentheses are the data used to calculate percentages.

category 4A (50% of all lesions), 16 as BI-RADS category 4B (17%), and seven as BI-RADS category 4C (7%). Twenty-five lesions (26%) were considered highly suspicious for malignancy (BI-RADS category 5). Forty-four women had a single lesion classified at standard US as BI-RADS category 4A, 13 as BI-RADS category 4B, six as BI-RADS category 4C, and 19 as BI-RADS category 5. One woman had two BI-RADS category 4A lesions, one had two BI-RADS category 4B lesions, one had a BI-RADS category 4A and a BI-RADS category 4B lesion, two women had two BI-RADS category 5 lesions, one had a BI-RADS category 5 and a BI-RADS category 4A lesion, and one had a BI-RADS category 5 and a BI-RADS category 4C lesion.

Pathologic analysis confirmed malignancy in 20 of the 25 BI-RADS category 5 lesions (80%), with fibrosis, fibroadenoma, and fibrocystic changes accounting for the five other diagnoses; surgical excision (n = 1), repeat biopsy (n = 3), and imaging follow-up (n = 4; range, 19–28 months) confirmed these benign diagnoses. Four malignancies were classified as BI-RADS category 4C (two infiltrating lobular carcinomas) or BI-RADS category 4B (two infiltrating ductal carcinomas). There were no malignancies within the 48 lesions classified as BI-RADS category 4A (Table 1). Among the 24 cancers, there were 22 infiltrating carcinomas (92%); most were infiltrating ductal carcinomas (n = 16), with three infiltrating lobular carcinomas, one mixed ductolobular malignancy, one tubular carcinoma, and one intrabreast metastasis of gynecologic origin. Two lesions were ductal carcinoma in situ at biopsy (8%), with stromal microinfiltration identified in one lesion at surgery.

Fibroadenomas accounted for 38 of the 72 benign lesions (53%), with fibrocystic changes accounting for 20 lesions (28%) (Table 2). Seven lesions were diagnosed as stromal fibrosis (10%), and five lesions were of papillary origin—one was associated with atypical ductal hyperplasia at surgery. The other two diagnoses were one radial scar and one angiolipoma.

STC Data Analysis

Analysis of data obtained with backscatter US demonstrated that the most discriminant parameter used to avoid biopsy was the supratumoral k value; the mean ± standard deviation measured 0.25 ± 0.15 in the benign lesions, compared with 0.33 ± 0.10 for the malignant lesions (P = .033). The intratumoral α value was 1.03 ± 0.85 for benign lesions compared with 0.69 ± 0.41 for malignant lesions (P = .067), while the infratumoral μ_n value was 28.7 ± 16.7 for benign lesions versus 23.2 ± 11.3 for malignant lesions (P = .209).

By considering the positive or negative offset on the mean of each parameter (ie, 2.94 multiplied by the standard deviation of each parameter), the thresholds used for classification of lesions were, on average, equal to 0.025, 1.89, and 56.4 over the 89 training sets of the cross-validation scheme for the supratumoral k value, intratumoral α value, and infratumoral μ_n value, respectively. Application of this model is illustrated in Figure 2.

STC Model Performance

The point of the ROC curve closest to the ideal classification scheme provided
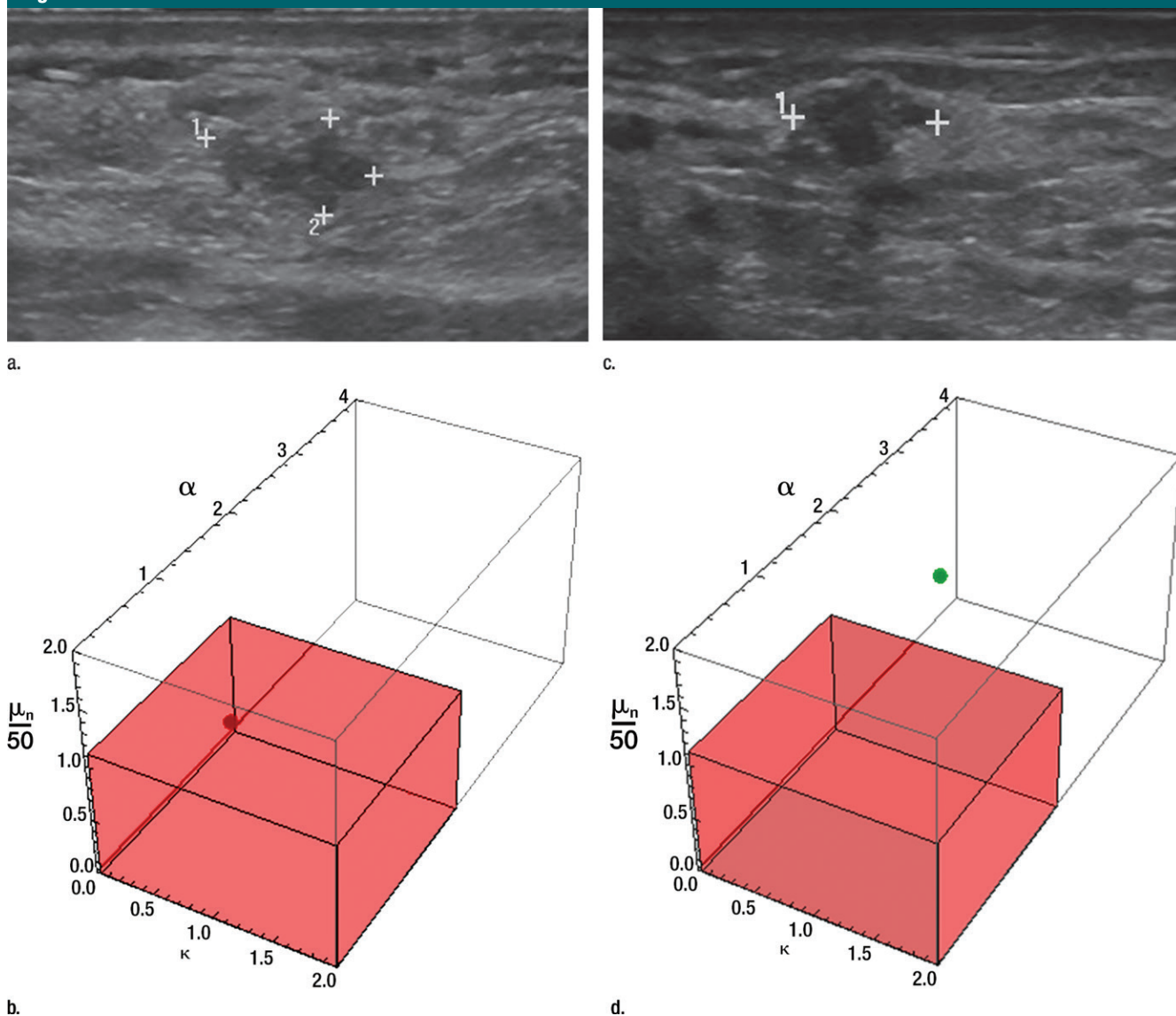
Figure 2: STC model classification is demonstrated after US evaluation of solid breast lesions. **(a)** B-mode US image obtained in a 37-year-old woman in whom a 9×5-mm ill-defined nodule was identified and estimated to be highly suspicious for malignancy (BI-RADS category 5). Final diagnosis after core-needle biopsy and surgery confirmed ductal carcinoma in situ, grade 2–3. **(b)** Schematic representation for the three parameters ($k = 0.2377$, $\alpha = 1.512$, $\mu_n = 22.10$) that correctly characterize the lesion as suspicious for malignancy, within the red box (based on $t = 2.94$). **(c)** B-mode US image obtained in a 65-year-old woman with an indeterminate 4-mm irregular nodule. It was classified as suspicious for malignancy (BI-RADS category 4C). Core-needle biopsy led to the diagnosis of a benign sclerosing lesion without atypia. **(d)** Schematic representation for the three parameters ($k = 0.3320$, $\alpha = 3.086$, $\mu_n = 44.33$) that correctly characterize the lesion as benign, outside the red box (based on $t = 2.94$).

a sensitivity of 79% and a specificity of 69%. The area under the ROC curve was 0.76 (Fig 3) (95% confidence interval: 0.65, 0.86) with a median of 0.77, as estimated with 2000 bootstrap sample data. A sensitivity of 100% (24 of 24 lesions) was obtained with $t = 2.94$ times the standard deviations of the parameters, which yielded a specificity of 24%. When analysis was performed on the subgroup of benign BI-RADS category 4A and 4B lesions, the specificity of this model increased to 26% (16 of 62 lesions), while maintaining 100% sensitivity. Four of these benign lesions belonged to two patients. For both of these patients, one lesion out of two was correctly classified as benign. Thus, 14 of 66 women (21%) with no confirmed malignant lesion
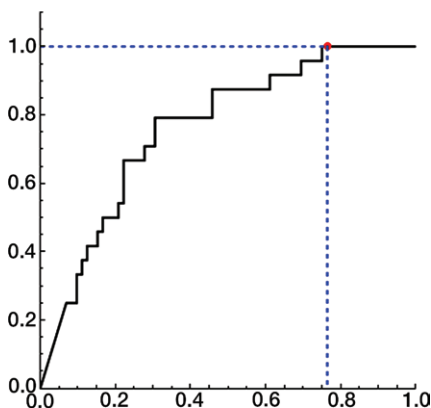
Radiology

Figure 3

Figure 3: ROC curve was obtained by varying the value of *t* (multiple of the standard deviations of the three parameters) and yielded an area under the curve of 0.76 (95% confidence interval: 0.65, 0.86). The value *t* = 2.94 (corresponding to a confidence level of 99.5%) offered sensitivity of 100% and specificity of 24% (1 − false-positive fraction).

would have avoided biopsy, and two of 66 (3%) would have avoided one of two biopsies. Two patients had a benign lesion (one was a BI-RADS category 4A lesion, the other a BI-RADS category 4C lesion) and a malignant lesion; none of these lesions were classified as benign according to the proposed STC method.

The assessment of the robustness of the proposed backscatter US method with manually drawn initial lesion contours yielded sensitivities of 96%, 100%, and 96% in BI-RADS category 4–5 malignant lesions and specificities of 24%, 21%, and 15% in BI-RADS category 4–5 benign lesions for random perturbations of contours within radii of 0.5, 1.0, and 1.5 mm, respectively. In BI-RADS category 4A–4B lesions, sensitivities remained at 100%, whereas specificities increased to 26%, 23%, and 18%, respectively.

Discussion

US characterization of solid lesions is based on well-defined morphologic criteria. Lesions with a probability of malignancy above 2%—BI-RADS category

4A and higher—are recommended to undergo biopsy to exclude cancer. We have developed a model based on statistical tissue characterization for the evaluation of solid breast lesions classified as BI-RADS categories 4–5 after clinical, mammographic, and standard B-mode US evaluation. With a sensitivity of 100%—no malignant lesion misclassified as benign—the proposed model yielded an overall specificity of 24%, with an area under the ROC curve of 0.76.

The performance of this model further improves when clinical suspicion of malignancy is taken into consideration. The model was most effective for BI-RADS category 4A and 4B lesions, with specificities of 23% (11 of 48 lesions) and 36% (five of 14 lesions), respectively, compared with specificities of 20% (one of five lesions) for BI-RADS category 4C lesions and 0% (zero of five lesions) for BI-RADS category 5 lesions. These results have much clinical relevance. Indeed, by excluding those lesions with a high a priori suspicion of malignancy on the basis of standard US morphologic characteristics (ie, BI-RADS category 4C and 5 lesions), where the radiologist is unlikely to forego the recommendation of biopsy verification to exclude malignancy, the specificity of the model increased to 26% (16 of 62 lesions). In our study population, this would translate to downgrading a quarter of the 62 benign lesions classified as BI-RADS category 4A and 4B to BI-RADS category 3, thus sparing 14 of 58 women (24%) biopsies to confirm benignity and sparing two of 58 women (3%) one of two biopsies.

Watching these lesions rather than sampling them at biopsy is akin to the approach described by Berg and coauthors (14) as they evaluated the performance of shear-wave elastography as an ancillary tool to characterize solid breast lesions at US. Within the constraint of 100% sensitivity, the six-point color score "E$_{col}$" of maximum elasticity at shear-wave elastography yielded a specificity of 34% (79 of 231 lesions) (14), and 79 benign lesions classified as BI-RADS category 4A could be downgraded on the basis of a specific feature

at shear-wave elastography, compared to 26% with our model (16 of 62 lesions).

By analyzing the work of other teams who used STC for lesion analysis and using ROC analysis at 100% sensitivity, we can estimate that Shankar et al (17) obtained specificities of 26% and 32% by using the *K* and Nakagami distribution models, respectively, to characterize 52 solid lesions. Combining the Nakagami distribution model with an image-compounding technique to improve the signal-to-noise ratio, the same team (18) obtained a specificity of 26%. Best results were obtained by combining five statistical parameters, with specificity increasing to 62% (19). Tsui et al (20) obtained a specificity of 27% by using the Nakagami distribution, increasing to 46% by also exploiting a geometric feature of lesion contours. However, comparison with these studies requires caution—first, because BI-RADS categories were not reported, and, thus, data on the performance of these methods for the evaluation of BI-RADS 4A–4B category lesions cannot be estimated—but, more important, because the testing set included the training set.

Subanalyses were performed to evaluate the performance of the STC model in classifying specific types of benign lesions. The model was used to correctly classify as benign 26% of confirmed fibroadenomas (10 of 38 lesions), 15% of fibrocystic changes (three of 20 lesions), and 43% of areas of fibrosis (three of seven lesions), lesions that are often challenging at standard US because of the shadowing and characteristic hypoechoic texture, which raise the suspicion for malignancy.

The results obtained are also plausible biologically. Malignant masses typically demonstrate spiculated margins, with a consequent expected increase in the parameter *k,* which reflects the cellular organization of the nuclei; a higher variability in cellular morphology, with a predicted decrease in α*,* a parameter that reflects cellular homogeneity; as well as posterior shadowing, resulting in an expected lower value of μ$_n$ in the infratumoral zone, a parameter related

to B-mode echogenicity. Indeed, these trends were observed in the comparison of malignant and benign lesions with the proposed method.

While these results are promising, they will require additional testing to validate the conclusions in a larger number of solid lesions, including a wide range of benign and malignant lesion types. Another limitation of this study is that a fixed setting was used by default with the Teratech US scanner during the cine sequences. A standardized acquisition protocol was chosen to reduce the effect of confounding factors that may affect the echo envelope statistics, such as the position and size of the focal zone, the transducer frequency, and the signal attenuation. Innovative solutions have since been published that aim to reduce the effect of some of these confounding factors (28,29) on STC classification strategies. Another potential limitation of our study is that one radiologist drew lesion contours; a sensitivity analysis, however, showed that the manually delineated lesion contours could be modified within a radius of 1.5 mm without substantial effect on the results.

In future work, as was performed in the study of Oelze et al (21) on mice mammary tumors, it would be interesting to combine the statistical parameters with other quantitative US measures—such as elasticity parameters—to test an increase of the classification power of the proposed method. Indeed, because K homodyne characterization and shear-wave elastography provide complementary assessment, with K homodyne characterization demonstrating cellular properties of breast lesions and shear wave elastography demonstrating the mechanical properties, it may be favorable to combine both approaches for a better assessment after BI-RADS classification. Further work could also be done to optimize the statistical parameters adopted here.

In conclusion, we have shown that statistical tissue characterization of solid breast lesions is possible and was used to correctly classify 17 of 72 solid benign lesions (24%) while not missing any of the 24 malignant lesions.

Furthermore, this method was used to correctly classify 16 of 62 benign lesions (26%) initially classified as BI-RADS category 4A and 4B, representing an important potential improvement in the management of these BI-RADS categories.

References

1. Stavros AT, Thickman D, Rapp CL, Dennis MA, Parker SH, Sisney GA. Solid breast nodules: use of sonography to distinguish between benign and malignant lesions. Radiology 1995;196(1):123–134.

2. D'Orsi CJ, Sickles EA, Mendelson EB, et al. ACR BI-RADS Atlas, Breast Imaging Reporting and Data System. Reston, Va: American College of Radiology, 2013.

3. Berg WA, Blume JD, Cormack JB, et al. Combined screening with ultrasound and mammography vs mammography alone in women at elevated risk of breast cancer. JAMA 2008;299(18):2151–2163.

4. Gokalp G, Topal U, Kizilkaya E. Power Doppler sonography: anything to add to BI-RADS US in solid breast masses? Eur J Radiol 2009;70(1):77–85.

5. Stuhrmann M, Aronius R, Schietzel M. Tumor vascularity of breast lesions: potentials and limits of contrast-enhanced Doppler sonography. AJR Am J Roentgenol 2000;175(6):1585–1589.

6. Raza S, Baum JK. Solid breast lesions: evaluation with power Doppler US. Radiology 1997;203(1):164–168.

7. Itoh A, Ueno E, Tohno E, et al. Breast disease: clinical application of US elastography for diagnosis. Radiology 2006;239(2):341–350.

8. Burnside ES, Hall TJ, Sommer AM, et al. Differentiating benign from malignant solid breast masses with US strain imaging. Radiology 2007;245(2):401–410.

9. Schaefer FKHI, Heer I, Schaefer PJ, et al. Breast ultrasound elastography—results of 193 breast lesions in a prospective study with histopathologic correlation. Eur J Radiol 2011;77(3):450–456.

10. Yoon JH, Kim MH, Kim EK, Moon HJ, Kwak JY, Kim MJ. Interobserver variability of ultrasound elastography: how it affects the diagnosis of breast lesions. AJR Am J Roentgenol 2011;196(3):730–736.

11. Bercoff J, Tanter M, Fink M. Supersonic shear imaging: a new technique for soft tissue elasticity mapping. IEEE Trans Ultrason Ferroelectr Freq Control 2004;51(4):396–409.

12. Athanasiou A, Tardivon A, Tanter M, et al. Breast lesions: quantitative elastography with supersonic shear imaging—preliminary results. Radiology 2010;256(1):297–303.

13. Tozaki M, Isobe S, Fukuma E. Preliminary study of ultrasonographic tissue quantification of the breast using the acoustic radiation force impulse (ARFI) technology. Eur J Radiol 2011;80(2):e182–e187.

14. Berg WA, Cosgrove DO, Doré CJ, et al. Shear-wave elastography improves the specificity of breast US: the BE1 multinational study of 939 masses. Radiology 2012;262(2):435–449.

15. Evans A, Whelehan P, Thomson K, et al. Quantitative shear wave ultrasound elastography: initial experience in solid breast masses. Breast Cancer Res 2010;12(6):R104–R114.

16. Shankar PM, Reid JM, Ortega H, Piccoli CW, Goldberg BB. Use of non-Rayleigh statistics for the identification of tumors in ultrasonic B-scans of the breast. IEEE Trans Med Imaging 1993;12(4):687–692.

17. Shankar PM, Dumane VA, Reid JM, et al. Classification of ultrasonic B-mode images of breast masses using Nakagami distribution. IEEE Trans Ultrason Ferroelectr Freq Control 2001;48(2):569–580.

18. Shankar PM, Dumane VA, Piccoli CW, Reid JM, Forsberg F, Goldberg BB. Classification of breast masses in ultrasonic B-mode images using a compounding technique in the Nakagami distribution domain. Ultrasound Med Biol 2002;28(10):1295–1300.

19. Shankar PM, Dumane VA, Piccoli CW, Reid JM, Forsberg F, Goldberg BB. Computer-aided classification of breast masses in ultrasonic B-scans using a multiparameter approach. IEEE Trans Ultrason Ferroelectr Freq Control 2003;50(8):1002–1009.

20. Tsui PH, Liao YY, Chang CC, Kuo WH, Chang KJ, Yeh CK. Classification of benign and malignant breast tumors by 2-D analysis based on contour description and scatterer characterization. IEEE Trans Med Imaging 2010;29(2):513–522.

21. Oelze ML, O'Brien WD Jr, Zachary JF. Quantitative ultrasound assessment of breast cancer using a multiparameter approach. In: IEEE Ultrasonics Symposium, 2007; 981–984.

22. Hruska DP, Oelze ML. Improved parameter estimates based on the homodyned K distribution. IEEE Trans Ultrason Ferroelectr Freq Control 2009;56(11):2471–2481.

23. Mamou J, Coron A, Oelze ML, et al. Three-dimensional high-frequency backscatter and envelope quantification of cancerous human lymph nodes. Ultrasound Med Biol 2011;37(3):345–357.

24. Destrempes F, Cloutier G. Review of envelope statistics models for quantitative ultrasound imaging and tissue characterization. In: Mamou J, Oelze ML, eds. Quantitative ultrasound in soft tissues. Dordrecht, the Netherlands: Springer, 2013; 219–274.

25. Kallel F, Bertrand M, Meunier J. Speckle motion artifact under tissue rotation. IEEE Trans Ultrason Ferroelectr Freq Control 1994;41(1):105–122.

26. Destrempes F, Meunier J, Giroux M-F, Soulez G, Cloutier G. Segmentation of plaques in sequences of ultrasonic B-mode images of carotid arteries based on motion estimation and a Bayesian model. IEEE Trans Biomed Eng 2011;58(8):2202–2211.

27. Destrempes F, Porée J, Cloutier G. Estimation method of the homodyned K-distribution based on the mean intensity and two log-moments. SIAM J Imaging Sci 2013;6(3):1499–1530.

28. Tsui PH, Yeh CK, Huang CC. Noise-assisted correlation algorithm for suppressing noise-induced artifacts in ultrasonic Nakagami images. IEEE Trans Inf Technol Biomed 2012;16(3):314–322.

29. Sheet D, Karamalis A, Eslami A, et al. Joint learning of ultrasonic backscattering statistical physics and signal confidence primal for characterizing atherosclerotic plaques using intravascular ultrasound. Med Image Anal 2014;18(1):103–117.